The dipole approximation method and its coupling with the regular boundary element method for efficient electrical impedance tomography

N.A. Gumerov, G.L. Chahine, A.G. Goumilevski
DYNAFLOW, INC.
7210 Pindell School Road, Fulton, Maryland 20759, U.S.A.
EMail: nail@dynaflow-inc.com

Abstract

The Electrical Impedance Tomography (EIT) utilizes CPU time-consuming minimization techniques for imaging an object. In this paper we present a computationally fast method for the forward/inverse EIT problem based on an asymptotic solution to Laplace's equation for an imaged domain with a small size inclusion situated inside of it. In this solution the principal term is represented by a dipole term. The computational time required by an EIT problem using the Dipole Approximation (DA) can be two orders of magnitude smaller than when using regular BEM. Results of numerical tests show a substantial improvement in the speed of the inverse problem solution when using the DA BEM approach.

1 Introduction

Imaging of the tissues inside the body as a diagnostic tool plays a vital role in modern medicine, and various technologies have been developed for this purpose including X-ray imaging, computerized tomography, gamma-ray densitometry, magnetic resonance imaging, and ultrasound techniques[1]. These techniques attempt to determine the internal structure of tissue by externally exposing the subject to some disturbance or excitation and by measuring the affected physical quantity. In Electrical Impedance Tomography (EIT) the distribution of conductivity inside an object is sought by applying specified currents (or voltages) at some parts of the object surface, and performing measurements of the voltage (or current) at other parts. The equations for the electric field then provide a relationship between the

conductivity distribution inside the object and the measured voltages and currents. Different types of materials have different conductivities, and the availability of a conductivity map provides an image of the material distribution. Schematic of the EIT procedure can be found elsewhere[1-4].

Since the mid 1980s EIT has seen intense research efforts to develop it into a useful technique for medical, two-phase flows, or other imaging. However, despite these efforts the technique still remains restricted to the laboratory, and to two-dimensional applications. The key reason is that computationally the problem of obtaining images from measurements requires extensive resources in computer memory and time. In the previous studies conducted at DYNAFLOW, INC. we have developed an efficient algorithm based on the Boundary Element Method[2-4]. The innovation in the present work is the use of asymptotic expansion based approximation, the Dipole Approximation (DA), to speed up the solution of the EIT problem.

2 Boundary Element Method

Consider a region of constant electrical conductivity σ_0 bounded by a boundary surface S. An electric current I is injected into this region through a pair of electrodes denoted by the symbols e_i (source) and e_j (sink), respectively. This is repeated using N combinations of electrodes. The injected electric current excites the electric potential, ϕ^{ij} satisfying the Laplace's equation and the following boundary conditions:

$$\nabla^2 \phi^{ij}(\mathbf{x},\mathbf{y}) = 0, \qquad i,j = 1,...,N, \qquad i \neq j, \tag{1}$$

$$\left.\frac{\partial \phi^{ij}}{\partial n}\right|_{\mathbf{x}\notin \mathbf{e}_i, \mathbf{x}\notin \mathbf{e}_j} = 0, \qquad \left.\frac{\partial \phi^{ij}}{\partial n}\right|_{\mathbf{x}\in \mathbf{e}_i} - - \left.\frac{\partial \phi^{ij}}{\partial n}\right|_{\mathbf{x}\in \mathbf{e}_j} = \frac{I}{\sigma_0}. \tag{2}$$

Equation (eqn 1) can be reformulated via Green's identity:

$$a\pi \phi^{ij}(\mathbf{x}) = \int_S \mathbf{n} \cdot \left[\phi^{ij}(\mathbf{y}) \nabla G(\mathbf{x},\mathbf{y}) - G(\mathbf{x},\mathbf{y}) \nabla \phi^{ij}(\mathbf{y})\right] dS, \tag{3}$$

where $a\pi$ is the angle in 2D (solid angle in 3D) under which the point $\mathbf{x}$ sees the rest of the domain, and G is the Green's function. The surface integrals can be performed by suitably discretizing the boundaries. In 2D we accomplish this by fitting cubic splines through known points on the boundary. Following a collocation approach, by selecting the points $\mathbf{x}$ to be the nodes on S, a linear system of equations of the form

$$\mathbf{A}\frac{\partial \phi^{ij}}{\partial \mathbf{n}} = \mathbf{B}\phi^{ij} \tag{4}$$

results. Here $\mathbf{A}$ and $\mathbf{B}$ are matrices corresponding to the discretization and integration with the Green's function and its derivative. On accounting for boundary conditions at the collocation points, one obtains a closed system of equations, which leads to ϕ^{ij} and $\partial \phi^{ij}/\partial n$ at the boundary.

3 Dipole Approximation

Consider an important practical case where L small objects of zero conductivity are located inside a domain of constant conductivity. Such case is typical of applications where small bubbles are situated in a flow or small size cracks are present in a domain. We decompose the potential ϕ^{ij} into

$$\phi^{ij} = \Phi_0^{ij} + \Phi^{ij}, \qquad i,j = 1,...,N, \qquad i \neq j \tag{5}$$

where Φ_0^{ij} is the undisturbed potential which can be found by solving the problem (eqn 1) in the domain D in the absence of objects and Φ^{ij} is the inclusion induced potential. ϕ^{ij} satisfies the same equation and boundary conditions at the outer boundary of the domain as Φ_0^{ij} plus conditions at the boundaries $s_1,...,s_L$ of the embedded small objects:

$$\left.\frac{\partial \phi^{ij}}{\partial n}\right|_{\mathbf{x}\in s_m} = 0, \qquad m = 1,...,L. \tag{6}$$

Subtracting the equations for Φ_0^{ij} from those for ϕ^{ij} we find that the induced potential, Φ^{ij}, can be obtained by solving the following problem:

$$\nabla^2\Phi^{ij} = 0, \quad \left.\frac{\partial \Phi^{ij}}{\partial n}\right|_{\mathbf{x}\in S} = 0, \qquad \left.\frac{\partial \Phi^{ij}}{\partial n}\right|_{\mathbf{x}\in s_m} = -\,\mathbf{n}\cdot\nabla\Phi_0^{ij}\Big|_{\mathbf{x}\in s_m}. \tag{7}$$

To exploit the fact that in many cases inclusions are small compared to the full domain we can use the method of matched asymptotic expansions[5] for solution of Problem (eqn 7). $\mathbf{U}_0^{ij}=\nabla\Phi_0^{ij}$ appears as a constant over the small inclusion when considering the domain scale. In the inner problem, at the scale of the inclusion we can determine Φ^{ij} from

$$\nabla^2\Phi^{ij} = 0, \qquad \Phi^{ij}\big|_{r_m\to\infty} = C_m^{ij}, \quad \left.\frac{\partial \Phi^{ij}}{\partial n}\right|_{\mathbf{x}\in s_m} = -\mathbf{n}\cdot\mathbf{U}_0^{ij}, \tag{8}$$

where $r_m = |\mathbf{r}_m|$ is the distance measured from the center of the mth inclusion and C_m^{ij} is a matching constant obtained from matching the inner solution with the outer solution:

$$\left(\Phi_{in}^{ij}\right)_{out} = \left(\Phi_{out}^{ij}\right)_{in}. \tag{9}$$

This problem is classical and corresponds to the velocity potential generated by a body moving with velocity $\mathbf{U}_0$ in an inviscid liquid. For a body of constant volume the principal terms of the asymptotic expansion at $r_m\to\infty$ are

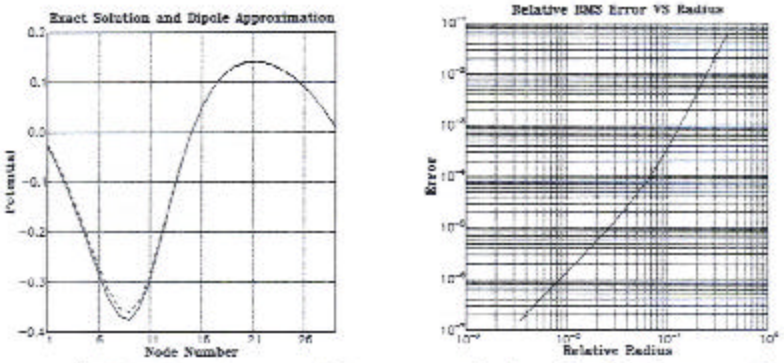

Figure 1: a) The electric potentials computed using the dipole approximation (solid line) and the BEM (dashed line). b) Dependence of the r.m.s. difference between these potential on the relative size of the imaged object (cylinder).

$$\Phi^{ij}\big|_{r_m\to\infty} = C_m^{ij} + \frac{\mathbf{M}_m^{ij}\mathbf{r}_m}{r_m^3} + O(r_m^{-3}), \text{ in the 3D case,} \tag{10}$$

$$\Phi^{ij}\big|_{r_m\to\infty} = C_m^{ij} + \frac{\mathbf{M}_m^{ij}\mathbf{r}_m}{r_m^2} + O(r_m^{-2}), \text{ in the 2D case,} \tag{11}$$

where $\mathbf{M}_m^{ij}$ is the dipole moment, depending on the body shape and orientation with respect to $\mathbf{U}_0$. For symmetrical bodies (sphere and circle of radius R_m) we have the following well-known expressions

$$\mathbf{M}_m^{ij} = \frac{1}{2}R_m^3\mathbf{U}_0^{ij}, \quad \text{in the 3D case,} \tag{12}$$

$$\mathbf{M}_m^{ij} = R_m^2\mathbf{U}_0^{ij}, \quad \text{in the 2D case.} \tag{13}$$

In the case of multiple bodies the principal terms become

$$\left(\Phi_{in}^{ij}\right)_{out} = C^{ij} + \sum_{m=1}^{L}\frac{\mathbf{M}_m^{ij}\mathbf{r}_m}{r_m^N} + ..., \text{ in the } N\text{-dimensional case.} \tag{14}$$

The outer solution has dipole singularities at the inclusion locations, $\mathbf{x} = \mathbf{x}_m$. In other words it satisfies the following Poisson equation:

$$\nabla^2\Phi^{ij} = -4\pi\sum_{m=1}^{L}\frac{\mathbf{M}_m^{ij}(\mathbf{x}-\mathbf{x}_m)}{|\mathbf{x}-\mathbf{x}_m|^N}, \quad \left.\frac{\partial\Phi^{ij}}{\partial n}\right|_{\mathbf{x}\in S} - 0. \tag{15}$$

Solution of this problem can be found using Green's identity:

$$a\pi\Phi^{ij}(\mathbf{x}) = a\pi \sum_{m=1}^{L} \frac{\mathbf{M}_m^{ij}\,(\mathbf{x}-\mathbf{x}_m)}{|\mathbf{x}-\mathbf{x}_m|^N} + \int_S \mathbf{n}\cdot\left[\Phi^{ij}(\mathbf{y})\nabla G(\mathbf{x},\mathbf{y})\right] dS. \qquad (16)$$

This equation clearly shows that the outer solution matches with the inner solution, (eqn 14) and (eqn 9).

4 Implementation of the DA

In this section we explain the implementation of the dipole algorithm and describe some computational results. To compute the dipole moment, $\mathbf{M}_m^{ij}$, one needs to evaluate the gradient of the undisturbed potential, $\nabla\Phi_0^{ij}$, at the location of the object. This can be accomplished by computing the potential at a set of points inside the computational domain with the help of Green's identity and by cubic spline-fit to the data. The spline fit involves computation of the second derivatives of the data while the first derivatives are evaluated by linear interpolation of the second ones[6]. Once the dipole moment has been computed, the induced potential is evaluated by solving a linear set of equations which are written at the collocation points. These equations result from discretization of (eqn 16) and have the form of (eqn 4). The resulting matrix $\mathbf{B}$ is singular; thus the solution to the equation is non-unique. We overcome this difficulty by the following way: one of the collocation points is assumed to be 'grounded', which removes the ambiguity of the potential.

Figure 1a illustrates an example of the computation of the distribution of the induced potential over the various node. 30 nodes were arranged in a clockwise direction; the node number fifteen was 'grounded'. The computed potential almost lies on top of the exact potential, Φ_k^{ij} . These plots correspond to the current 'sink' located at node # 8 , and current 'source' at node # 23. The difference in potentials are largest at the nodes situated closer to the cavity center. These calculations were done for a circular cavity with coordinates $(7,-3)$ and radius, $R = 5$, located inside a circle with radius, $R_o = 30$, and centered at $(0,0)$. We repeated the calculations for the same location of cavity, but with different radii. Figure 1b depicts the r.m.s. deviation of the induced electrical potential versus the relative radii of the cavity, R/R_o. At small values of the relative radii the error scales as the radius squared, in accordance with (eqn 10). As the size of the cavity is increased, the value of the error increases and, at $R/R_o = 0.25$ the relative error is about one percent. Therefore, the dipole approximation is a 'good' one for objects with relative radii, say, less than one tenth of the domain characteristic length while for larger objects the accuracy of the dipole approximation suffers.

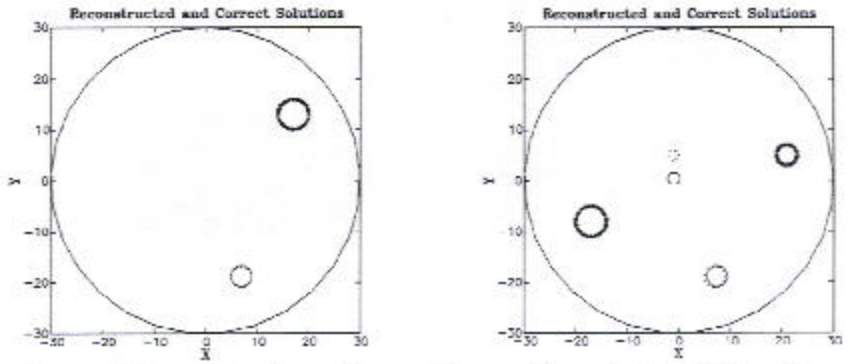

Figure 2: Reconstruction of the position and size of a single (a) and two (b) inclusions using the dipole method. The initial guess is shown by the stars, while the reconstructed and correct images are plotted by the solid and dashed lines, respectively.

5 Inverse Problem

To solve an inverse EIT problem one needs to apply a concept of minimization. We thus introduce an objective function:

$$F(\mathbf{p}) = \frac{1}{\|U\|}\sqrt{\sum_{i=1}^{N}\sum_{j=i+1}^{N}\sum_{\substack{k=1\\k\neq i,j}}^{N}\left[\phi_k^{ij}(\mathbf{p}) - U_k^{ij}\right]^2}, \tag{17}$$

where $\mathbf{p} = (p_1, p_2, ..., p_{N_p})$ is the parametrization vector, N_p is the number of parameters, and ϕ_k^{ij} are U_k^{ij} are the computed and measured voltages at the kth electrode corresponding to the ith and jth excitation electrodes.

Parametrization of a conductivity distribution in a given domain can be made by many ways. For example an inclusion of a material of a different conductivity than the host medium in a 2D configuration can be represented by $N_p - 3$ parameters, α_k, of an expansion in addition to 3 parameters for the center position and the reference angle, θ_0:

$$r(\theta - \theta_0) = \sum_{k=1}^{N_p-3} \alpha_k \mathcal{P}_{k-1}(\cos(\theta - \theta_0)), \tag{18}$$

where r is the distance from a selected point (x_0, y_0) inside the body to the boundary, θ is the polar angle of the point on the body, and $\mathcal{P}_k$ are the Legendre polynomials. The space of parameters consists of x_0, y_0, θ_0 and the $N_p - 3$ coefficients α_k.

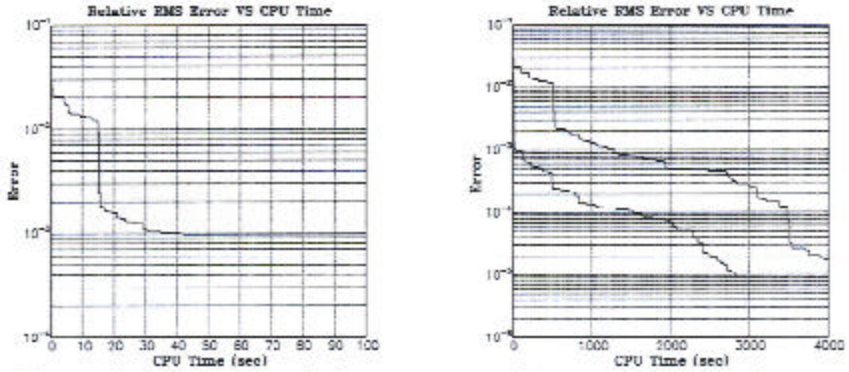

Figure 3: Dependence of the r.m.s. error between correct and reconstructed solution on the CPU time (SGI Indigo 2). The forward problem solver is based on the DA (a), BEM (the upper curve b), and the combination of the DA and the BEM (the lower curve b).

The inverse problem solver based on the DA is very efficient because the BEM calculation is performed only once – during the first call. The computation of the interpolation coefficients to determine the gradient of the undisturbed field is time consuming but also is performed only once. Moreover, the interpolation coefficients and the LU-decomposed matrix $\mathbf{B}$ are computed once for the prescribed geometry and are stored for subsequent steps.

To test the feasibility of the dipole algorithm we employed Powell's algorithm[6]. By minimizing the objective function with respect to $\mathbf{p}$, we are able to reconstruct the location and the size of the objects. An example of reconstruction of the position and size of a single cylindrical inclusion with zero conductivity is shown in the left Figure 2. The location of the center of the cavity and its radius are recovered fast with an accuracy of about one percent. The right Figure 2 shows another example were we reconstructed the shape of two cavities. The CPU time needed to minimize the objective function is shown in Figure 3a. These calculations were performed on an SGI Indigo II workstation. At the computational time of about fifty seconds Powell's algorithm reached a local minimum of the objective function and the r.m.s. error leveled off for the initial guess used. We would like to emphasize that the dipole method is an approximation. Therefore, the r.m.s. error does not converge to zero as it is expected to in the case of the application of minimization routines using the BEM[3,4].

6 Coupling of the Dipole and the BEM Codes

To reduce the total CPU time one can employ the dipole algorithm to obtain an initial guess for the BEM, then continue with the more accurate BEM. Figure 3b shows a comparison of the CPU time required by the Powell's

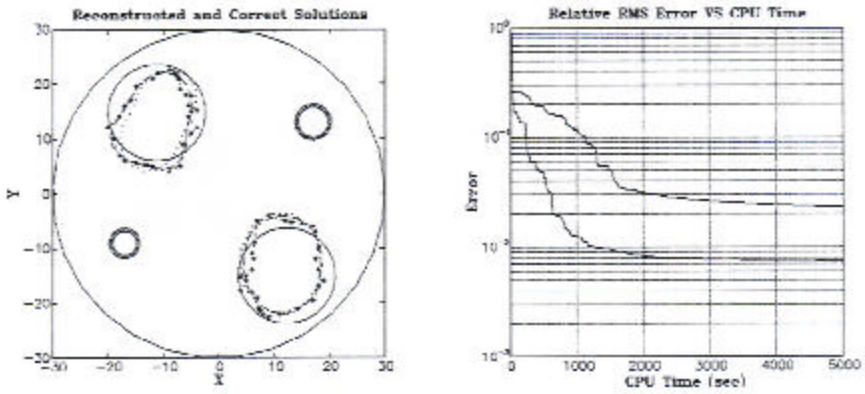

Figure 4: a) Shape reconstruction of two objects shown by the stars. The initial guess is shown by the circled lines. The solutions obtained using the DA and BEM methods are represented by the solid and dotted lines, respectively. The dashed lines illustrate the solution obtained using the combination of the DA and the BEM. The lower curve (b) shows the convergence steps for the later case. The upper curve (b) corresponds to reconstruction based on the BEM.

algorithm using BEM during the full computation and that starting with the aid of the DA and continued using the BEM[3,4]. One should notice that the combination of the two approaches allows to reduce the computational time by about fifty percent.

Figure 4a shows a further attempt at deducing the shape of two inclusions with the aid of the Powell minimization using the DA and the BEM[3,4].

The later was started with the same guess to provide an initial guess for the BEM. In the BEM implementation the shape of each cavity was approximated by applying seven Legendre polynomials. The comparison of the required CPU time for these two cases again shows significant reduction of the computational time (Figure 4b).

These examples demonstrate the capability of the dipole method to obtain the initial guess required by the algorithm based on the BEM. This initial guess is relatively close to the correct solution and results in CPU time reduction. Further improvements may be achieved if one introduces for non-spherical bodies quadrupole or higher order approximations to the solution.

7 Influence of Noise

The examples shown so far assumed experimental data with no errors. However, experimental measurements always have some component of errors. An important question is to what extent minimization algorithms using the

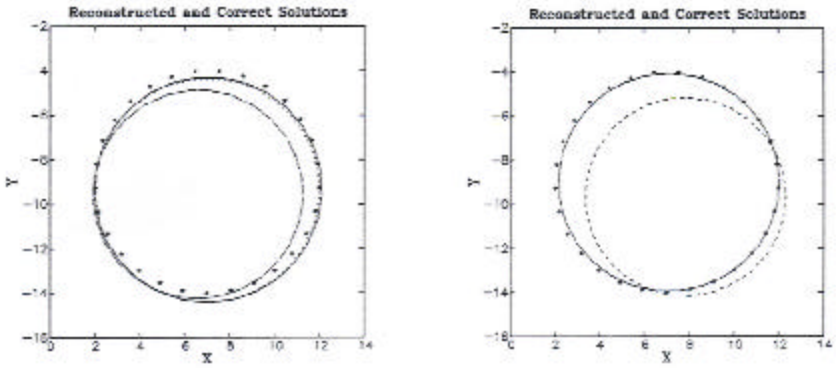

Figure 5: Reconstruction of a circle shown by stars using the dipole method (the left figure) and the BEM based Powell algorithm. The solid, dotted, and dash-dotted lines show the solution corresponding to experimental data truncated to three, two, and one digits. For the case represented on the right figure the solution converged to a circle with zero radius (it is not shown) when we kept only one digit.

BEM and the dipole approximation are sensitive to errors in the experimental measurements. To answer this question we made a series of simulations where experimental noise was modeled by using input data with different degrees of accuracy. This degree of accuracy was selected by keeping only a finite number of digits in the representation of the experimental data and disregarding the rest. This model of noise reflects the finite accuracy of instruments in recording experimental measurements. We report first data of simulations done with the aid of the dipole algorithm, and then we report data related to the BEM and show the influence of this noise on the reconstructed solutions.

Figure 5 left illustrates an example of the converged and correct solutions in the case of one cylindrical inclusion inside a cylindrical container. Here we plotted the shape of the inclusion only. The solid, dotted, and dashed-dotted lines show the solutions obtained by keeping only three, two, and one significant digits in the numerical representation of the experimental data, while the stars show the exact solution. As the accuracy of the experimental data worsens, the reconstructed shape deviates more from the correct one. These converged solutions were then used as initial data for the BEM based code[3,4] to continue the convergence procedure. The dipole approximation to the solution neglects higher order terms in the representation of the true solution. Figure 5 right illustrates the converged and correct solutions obtained with the aid of the BEM based algorithm. A comparison of the results of computations done with the help of the DA and the BEM based algorithms shows that the BEM is more accurate if we keep three and more digits in the representation of experimental data while, on the

contrary, the DA performs better if we keep two or less digits. For one digit data representation, the BEM algorithm predicts a cavity which contracts to a point with zero radius while, the dipole algorithm still gives a reasonable solution. Therefore, to recover the size and the shape of cavities with the aid of the BEM based method the measurements error should be less than one percent. If the measured data are less accurate the dipole method is much superior.

8 Conclusions

In the work described here we implemented the DA for EIT problem. This drastically reduces the required computational time and allows implementation of efficient minimization strategies. We also studied the influence of noise on the performance of the algorithm. Results showed stability of the reconstruction methods using BEM up to noise levels of 1% and stability of the dipole algorithm up to noise levels of 10%. This characterizes the dipole method and its coupling as robust and practical.

References

[1] Webster, J.G. Electrical impedance imaging, in *Electrical Impedance Tomography*, J.G. Webster (ed.), Adam Hilger, New York, 1990.

[2] O'Hern, T.J., Torczynski, J.R., Ceccio, S.L., Tassin, A.L., Chahine, G.L., Duraiswami R. & Sarkar, K., Development of an electrical impedance tomography system for an air-water vertical bubble column, in *Forum on Measurement Techniques in Multiphase Flows*, FED-**233**, ASME, New York, pp. 531-537, 1995.

[3] Duraiswami R., Chahine G.L. & Sarkar K., Boundary Element Technique for Efficient 2-D and 3-D Electrical Impedance Tomography, *Chemical Engineering Science*, **52**(13), pp. 2185-2196, 1997.

[4] Duraiswami, R., Sarkar, K. & Chahine, G.L., Efficient 2D and 3D electrical impedance tomography using dual reciprocity boundary element techniques, *Engineering Analysis with Boundary Elements*, **22**, pp. 13-31, 1998.

[5] Nayfeh, A.H., *Introduction to Perturbation Techniques*, John Wiley & Sons, 1981.

[6] Press, W.H., Teukolsky, S.A.,Vetterling, W.T. & Flannery, B.P. *Numerical Recipes*, Cambridge University Press, 2nd ed., 1992.